

Perceptual Quality Assessment of Virtual Reality Videos in the Wild

Wen Wen¹ · Mu Li² · Yiru Yao³ · Xiangjie Sui³ · Yabin Zhang⁴ · Long Lan⁵ · Yuming Fang³ · Kede Ma¹

Abstract Investigating how people perceive virtual reality videos in the wild (i.e., those captured by everyday users) is a crucial and challenging task in VR-related applications due to complex *authentic* distortions localized in space and time. Existing panoramic video databases only consider synthetic distortions, assume fixed viewing conditions, and are limited in size. To overcome these shortcomings, we construct the VR Video Quality in the Wild (VRVQW) database, which is one of the first of its kind, and contains 502 user-generated videos with

Wen Wen
E-mail: wwen29-c@my.cityu.edu.hk

Mu Li (Corresponding author)
E-mail: limuhit@gmail.com

Yiru Yao
E-mail: yaoyiru1998@foxmail.com

Xiangjie Sui
E-mail: suixiangjie2017@163.com

Yabin Zhang
E-mail: zhan0398@e.ntu.edu.sg

Long Lan
E-mail: long.lan@nudt.edu.cn

Yuming Fang
E-mail: fa0001ng@e.ntu.edu.sg

Kede Ma
E-mail: kede.ma@cityu.edu.hk

¹ Department of Computer Science, City University of Hong Kong, Kowloon, Hong Kong

² School of Computer Science and Technology, Harbin Institute of Technology, Shenzhen 518055, Guangdong, China

³ School of Information Management, Jiangxi University of Finance and Economics, Nanchang 330032, Jiangxi, China

⁴ Multimedia Lab, Bytedance Inc.

⁵ Institute for Quantum Information & State Key Laboratory of High Performance Computing, College of Computer Science and Technology, National University of Defense Technology, Changsha 410073, Hunan, China

diverse content and distortion characteristics. Based on VRVQW, we conduct a formal psychophysical experiment to record the scanpaths and perceived quality scores from 139 participants under two different viewing conditions. We provide a thorough statistical analysis of the recorded data, observing significant impact of viewing conditions on both human scanpaths and perceived quality. Moreover, we develop an objective quality assessment model for VR videos based on pseudocylindrical representation and convolution. Results on the proposed VRVQW show that our method is superior to existing video quality assessment models, only underperforming viewport-based models that otherwise rely on human scanpaths for projection. Last, we explore the additional use of the VRVQW dataset to benchmark saliency detection techniques, highlighting the need for further research. We have made the database and code available at <https://github.com/limuhit/VR-Video-Quality-in-the-Wild>.

Keywords Virtual reality · Panoramic videos · Video quality assessment · Psychophysics

1 Introduction

As virtual reality (VR) acquisition and display systems become widely accessible, people are getting used to capturing, editing, and interacting with VR content, which is evidenced by the accelerated proliferation of panoramic videos¹ uploaded to popular video sharing and social media platforms (e.g., Bilibili and Youtube). A practical issue arising from panoramic videos in the wild is that they are often born with complex visual artifacts (i.e., the so-called *authentic* distortions) due to

¹ In this paper, we use the terms “panoramic”, “VR”, “360°”, “omnidirectional”, and “spherical”, interchangeably.

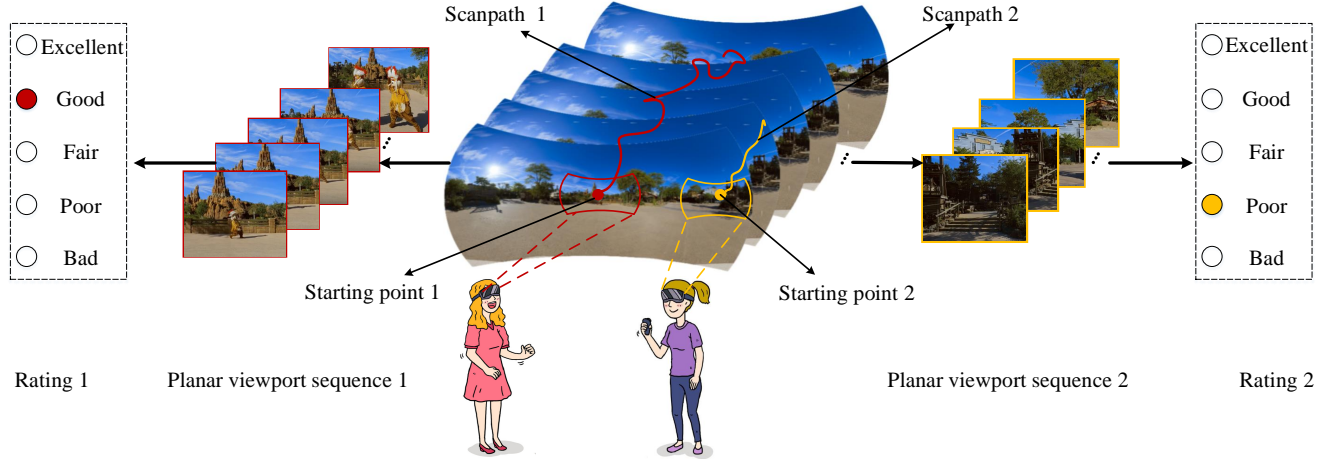


Fig. 1: Illustration of how people explore virtual reality (VR) videos in the proposed VRVQW database. Under varying viewing conditions (e.g., starting points and exploration times), users may exhibit different viewing behaviors in the form of scanpaths, leading to different portions of the video being explored. As user-generated VR videos often come with localized authentic distortions, the perceived quality may vary with user viewing behaviors constrained by viewing conditions. Therefore, the incorporation of viewing conditions would be the key to the success of computational quality prediction of user-generated VR videos.

scene complexity, lens imperfection, sensor limitation, non-professional shooting, and stitching inaccuracy. The acquired videos may subsequently undergo several stages of processing, including compression, editing, transmission, and transcoding, leading to additional video impairments (Azevedo et al., 2020). Understanding how people perceive 360° video distortions in virtual environments is central to many VR-enabled video applications.

Different from a planar video, a panoramic video, by its name, records/generates the scene of interest by capturing/tracing light from all directions at possibly varying viewpoints through time. This gives rise to a $360^\circ \times 180^\circ$ spherical field of view (FoV) at any time instance. With the help of a head-mounted display (HMD), users can freely explore the virtual scene using head and gaze movements as if they were in the real world. Such immerse and interactive viewing experience poses a great challenge to existing quality assessment methods for planar videos (Wang et al., 2004, 2012; Xu et al., 2020; Li et al., 2019b; Korhonen, 2019; Ying et al., 2021; Götz-Hahn et al., 2021) when predicting 360° video quality. Although several subjective quality studies (Singla et al., 2017; Curcio et al., 2017b; Tran et al., 2017; Duan et al., 2017; Zhang et al., 2017, 2018a; Lopes et al., 2018; Li et al., 2018; Meng and Ma, 2022) on panoramic videos have been conducted, they may suffer from three limitations. First, most of the resulting databases contain *synthetic* distortions only, with compression artifacts being the most representative. This is an oversimplification of the real-world

situation, where user-generated 360° videos may suffer from commingled *authentic* distortions, often *localized* spatiotemporally. The extensively studied compression artifacts may no longer dominate the perceptual quality. Second, the databases assume the viewing conditions such as the starting point and the exploration time to be fixed, which is overly restrictive when viewing virtual scenes with HMDs. Relaxing these constraints can lead to situations where the visible distortions of a 360° video are probably not perceived for some viewing conditions. Thus it is reasonable to rate the perceptual quality as high. Third, given a fixed human labeling budget, the number of unique reference 360° videos in the databases is determined by the number of synthetic distortion types and levels, which is limited to a few dozen (if not fewer). As such, these databases fail to sufficiently represent real-world videos with diverse content, distortion, and motion complexities.

Considering the aforementioned limitations of existing 360° video databases, several significant aspects related to understanding the perceptual quality of 360° videos remain unexplored. For example, how consistent are human behaviors under the same viewing condition? How are human behaviors affected by viewing conditions? How does perceived quality change with viewing conditions? Can we make effective computational quality predictions under different viewing conditions? In an attempt to answer these questions, we establish a large 360° video database called the VR Video Quality in the Wild (VRVQW) database. VRVQW comprises

Table 1: Summary of VR VQA databases. ERP, RCMP, and TSP stand for the equirectangular projection, the reshaped cubemap projection, and the truncated square pyramid projection, respectively. The numbers in the “#videos” column are in the form of “#reference videos / #distorted videos”.

| Database | Year | Projection | #videos | #subjects | Resolution | Duration (sec) | HM/EM data | Distortion type |
|-----------------------|------|----------------|----------|-----------|--------------------------------|----------------|------------|---|
| Singla et al. (2017) | 2017 | ERP | 6 / 60 | 30 | 1,920 × 1,080 to 3,840 × 2,160 | 10 | HM | H.265 compression, Downsampling |
| Curcio et al. (2017b) | 2017 | ERP | 3 / 24 | 12 | 3,840 × 1,920 | 21 | HM | Tile-based H.265 compression |
| Tran et al. (2017) | 2017 | ERP | 3 / 60 | 37 | 1,440 × 720 to 3,840 × 1,920 | 30 | N/A | H.264 compression |
| Duan et al. (2017) | 2017 | ERP | 10 / 150 | 13 | 4,096 × 2,048 | 15 | N/A | MPEG-4 compression, Downsampling |
| Zhang et al. (2017) | 2017 | ERP | 16 / 384 | 23 | 4,096 × 2,048 | 10 | N/A | H.264 compression H.265 compression, VP9 compression, Simulated packet loss |
| Zhang et al. (2018a) | 2018 | ERP | 10 / 50 | 30 | 3,600 × 1,800 | 10 | N/A | H.265 compression, Downsampling |
| Lopes et al. (2018) | 2018 | ERP | 6 / 79 | 37 | 960 × 480 to 7,680 × 3,840 | 10 | N/A | H.265 compression, Downsampling |
| Li et al. (2018) | 2018 | ERP, RCMP, TSP | 60 / 540 | 221 | 3,840 × 1,920 to 7,680 × 3,840 | 10 to 23 | HM + EM | H.265 compression, Projection |
| Meng and Ma (2022) | 2021 | ERP | 18 / 774 | 160 | 3,840 × 1,920 | 10 | N/A | H.264 compression, Downsampling |
| VRVQW (Proposed) | 2021 | ERP | – / 502 | 139 | 1,280 × 720 to 5,120 × 2,560 | 15 | HM + EM | Authentic distortion |

502 panoramic video sequences that cover a wide range of scenes, including cityscape, landscape, shows, sports, and computer-generated (CG) content. The videos also exhibit a wide range of complex authentic distortions, covering the full quality spectrum. To evaluate the subjective quality of a panoramic video as a function of viewing conditions, we invite subjects to watch the video from different starting points and time durations (see Fig. 1). A total of 40,268 human opinion scores, along with scanpaths (as viewing behaviors) from 139 users, are recorded. We then provide an in-depth analysis of our data, investigating the impact of viewing conditions on viewing behaviors and perceived quality.

Moreover, we take initial steps toward blind objective video quality assessment (VQA) of VR content. To respect the spherical nature of VR videos while maintaining a manageable computational budget, we resort to the pseudocylindrical representation (Li et al., 2021) in place of and as a generalization of the default equirectangular projection (ERP) format. On top of it, we design a lightweight convolutional neural network (CNN) for 360° VQA, in which the main operation—pseudocylindrical convolution—is fully compatible with the pseudocylindrical representation, and can be efficiently implemented by standard 2D convolution. We explicitly incorporate two viewing conditions—the starting point and the exploration time—into the model design by rotating the initial pseudocylindrical representation and adjusting the sampling rate, respectively. Experimental results show that our method effectively addresses the unique VQA challenges presented in the proposed VRVQW database, and performs favorably against existing methods. We additionally explore the use of VRVQW in benchmarking saliency detection methods, which reveals a significant room for improvement.

In summary, our main contributions are:

- a first-of-its-kind 360° video database, VRVQW, with complex authentic distortion,
- a carefully designed psychophysical experiment to record human scanpaths and quality scores under two viewing conditions, accompanied by thorough statistical analysis,
- a lightweight blind VQA model specifically for VR videos, aware of viewing conditions,
- a benchmark test of existing saliency detection methods in virtual environments.

2 Related Work

In this section, we detail the current landscape of 360° video quality assessment (VQA) databases with mean opinion scores (MOSs). We next review objective VQA models that have either been adapted or specifically designed to evaluate VR content. Lastly, we summarize current 360° saliency detection models.

2.1 Subjective Quality Assessment of Panoramic Videos

Singla et al. (2017) constructed one of the first databases to study the impact of H.265 compression and spatial resolution on 360° video quality. The database contains six reference videos and 60 distorted videos at two resolutions and five bitrates. Curcio et al. (2017b) performed a subjective user study of 360° videos under the tile-based streaming setting (Graf et al., 2017). The visual stimuli consisted of 24 distorted videos at four quality levels and two resolutions, carefully selected to probe whether the background tile should be encoded with higher resolution or higher fidelity given the same bitrate budget. Tran et al. (2017) established a small database containing 60 mobile distorted videos at five levels of H.264 compression and four resolutions. Duan et al. (2017)

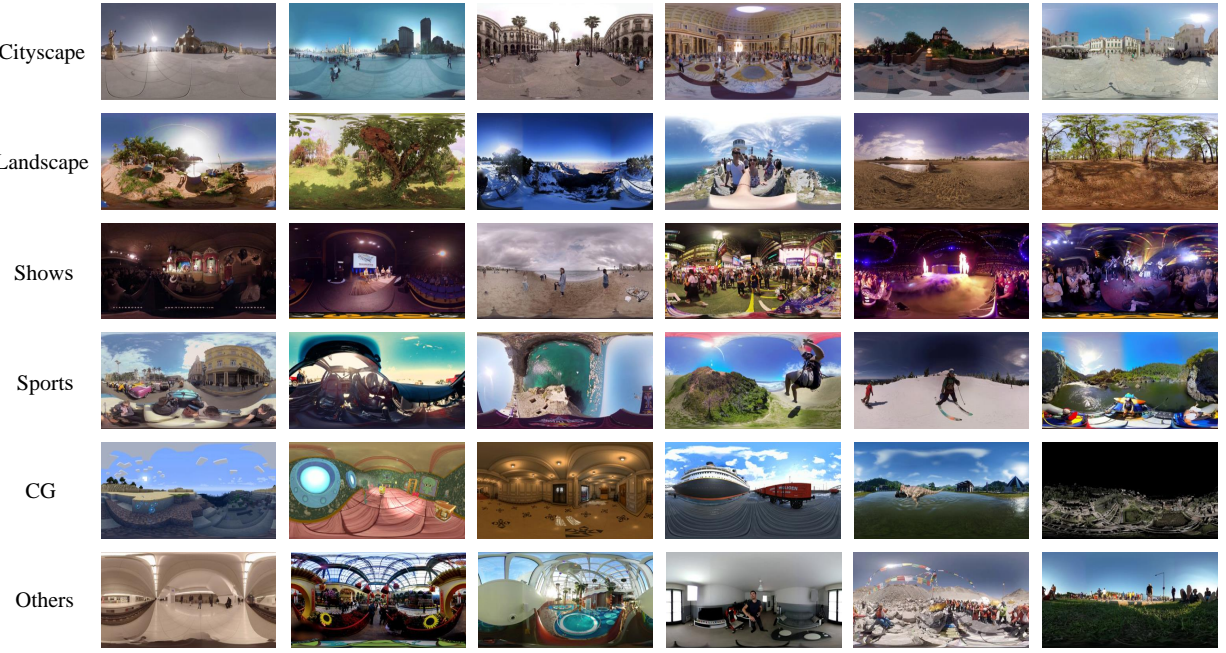


Fig. 2: Thumbnails of user-generated 360° video sequences in the proposed VRVQW database.

studied the impact of MPEG-4 compression and spatial resolution on the perceptual quality of 360° videos. Zhang et al. (2017) proposed a large omnidirectional video dataset, including 16 reference and 384 distorted videos, covering H.264, H.265, VP9 compression, and simulated packet loss. They also proposed a standardized subjective procedure with improved efficiency. Zhang et al. (2018a) conducted a comprehensive study on the interaction between subsampling and H.264 compression to panoramic video quality. They computed an optimal resolution, $3,600 \times 1,800$, for the HTC VIVE display. Lopes et al. (2018) studied the individual and combined effects of spatial resolution, frame rate, and H.265 compression to 360° videos. Li et al. (2018) introduced the VQA-ODV dataset, consisting of 540 impaired 360° videos from 60 references using different levels of H.265 compression and map projections. VQA-ODV also includes head movement (HM) and eye movement (EM) data, along with an analysis of human behavior consistency. VOD-VQA (Meng and Ma, 2022) is currently the largest panoramic video database, which includes 18 reference videos divided into two groups, resulting in a total of 774 distorted videos with different compression levels, spatial resolutions, and frame rates.

We present a summary of existing 360° video databases in Table 1, where we observe that these databases primarily consist of *synthetic* distortions, assuming the availability of original undistorted videos for database construction and model development. In

contrast, our focus lies on user-generated panoramic videos in the wild, many of which suffer from *authentic* distortions during video acquisition. Moreover, it is not uncommon to see that these distortions are *localized* in space and time, making viewing conditions indispensable for determining VR video quality (Sui et al., 2021).

2.2 Objective Quality Assessment of Panoramic Videos

Existing objective models for evaluating panoramic content are mainly adapted from planar image quality assessment (IQA) and VQA methods, applied to one of three data formats: (projected) 2D plane, spherical surface, and (projected) rectilinear viewport.

Methods in the planar domain (Sun et al., 2017; Zakharchenko et al., 2016; Kim et al., 2019b) aim to compensate for the non-uniform sampling caused by the sphere-to-plane projection. When using ERP, planar IQA/VQA methods can be enhanced by incorporating latitude-dependent weighting schemes. Another approach is to use the Craster parabolic projection to ensure uniform sampling density (Zakharchenko et al., 2016). Kim et al. (2019b) explored an adversarial loss for learning patch-based quality estimators using content and position features. Li et al. (2018) trained a CNN for panoramic video quality assessment, leveraging the HM and EM data. Methods in the spherical domain (e.g., S-PSNR (Yu et al., 2015b) and S-SSIM (Chen et al., 2018)) calculate and aggregate local quality esti-

mates over the sphere. Yu et al. (2015b) incorporated importance weighting derived from the empirical distributions of HM and EM data. Methods in the viewport domain focus on extracting viewports that are likely to be seen for quality computation. Xu et al. (2021) used graph convolutional networks to model the spatial relations of extracted viewports, which, however, does not necessarily reflect the human viewing process. Li et al. (2019a) proposed a two-stage approach, involving viewport proposal and quality assessment with spherical convolution (Cohen et al., 2018). Recently, Sui et al. (2021) suggested converting a panoramic image to planar videos by sampling sequences of rectilinear projections of viewports along users' scanpaths. This approach allows mature planar IQA/VQA methods to be directly applied.

2.3 Saliency Detection of Panoramic Videos

Panoramic video saliency detection aims to predict objects/regions of interest in VR environments. It identifies visually important information in panoramic videos and plays a key role in panoramic video streaming and rendering. Saliency detection is also crucial for visual quality assessment (Li et al., 2018; Yu et al., 2015b; Li et al., 2019a).

Current saliency detection methods for 360° videos can be divided according to their operating domain: (projected) 2D plane, spherical surface, and (projected) rectilinear viewport. Most panoramic saliency detection algorithms are built upon traditional planar methods while considering specific properties of the 2D projection (Nguyen et al., 2018; Cheng et al., 2018; Xu et al., 2019). Nguyen et al. (2018) proposed PanSalNet by fine-tuning a planar image saliency detector on two 360° video databases (Corbillon et al., 2017; Wu et al., 2017). Cheng et al. (2018) trained a CNN-based saliency detection model for 360° videos with a cube padding trick to alleviate projection distortions and boundary discontinuities. Xu et al. (2019) predicted HM positions in 360° videos based on deep reinforcement learning. In the spherical domain, Bogdanova et al. (2008) extended the classic saliency model (Itti et al., 1998) by extracting and combining intensity, chroma, and orientation features from the spherical Gaussian pyramid. Zhang et al. (2018b) proposed the spherical U-Net for saliency detection, where the translation of the convolution kernel becomes kernel rotation on the sphere. In the viewport domain, Lebreton and Raake (2018) extracted features from viewports based on orientation analysis, which were back-projected to the ERP domain. Concurrently, Lebreton et al. (2018) extended BMS360 (Lebreton and

Raake, 2018) to V-BMS360, enabled by the optical flow-based motion detection. A recent subjective user study on stereoscopic 360° images (Sitzmann et al., 2018) suggests a weak effect of viewing conditions on the gathered saliency maps. However, these results may no longer be valid in the context of user-generated 360° videos, which are thoroughly analyzed in the paper.

3 Subjective Quality Assessment of VR Videos in the Wild

In this section, we summarize our effort toward creating the VRVQW database that contains human perceptual data - MOSs and scanpaths by recording users' responses when watching 360° videos under different viewing conditions.

3.1 Data Gathering

3.1.1 Visual Stimuli

The VRVQW database contains 502 unique user-generated 360° video sequences, with frame rates ranging from 20 to 60 frames per second (fps) and resolutions ranging from $1,280 \times 720$ to $5,120 \times 2,560$ pixels. All videos were collected from the Internet and carry Creative Commons licenses. Each video is cropped to a duration of about 15 seconds and stored in the ERP format without further compression. VRVQW mainly includes 360° videos shot by a (nearly) static camera to reduce the probability of causing dizziness (Kim et al., 2019a), which could potentially affect the reliability of the collected MOSs. We only select 32 videos with significant camera motion, ensuring visual comfort through a posteriori questionnaire (Kennedy et al., 1993). These moving-camera videos typically receive a considerable number of likes on video-sharing platforms, and provide users with a stronger sense of immersion and interaction.

The video selection process aimed to encompass a range of scenes suitable for VR shooting, including *Cityscape*, *Landscape*, *Shows*, *Sports*, *CG*, and *Others* (refer to Fig. 2). *Cityscape* contains different places of interest around the world like the Roman Colosseum and other renowned historical sites. *Landscape* includes beautiful natural scenes, such as waterfalls, mountains, volcanoes, etc. *Shows* represent different forms of entertainment, including band performance, living theatre, and street improvisation. *Sports* gather various sporting events, e.g., car racing, skiing, and riding. *CG* is a collection of rendered videos by mature computer graphics techniques. Finally, the *Others* category is reserved for scenes that do not belong to the previous five classes.

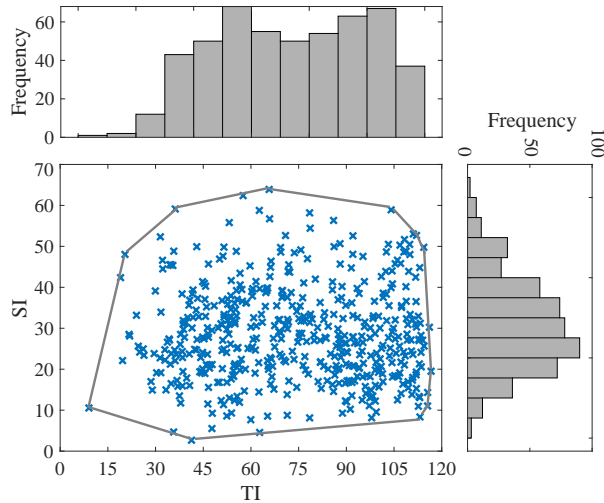


Fig. 3: Empirical distribution of 360° videos (denoted by blue crosses) in the SI-TI space with the fitted convex hull and 1D histograms.

As suggested by Winkler (2012), we quantify the content diversity of VRVQW using two low-level statistics: spatial information (SI) and temporal information (TI), with higher values indicating more complexities. Fig. 3 shows the 2D scatter plot together with 1D histograms, from which we see that the selected stimuli provide fairly wide coverage in the SI-TI space.

Different from existing 360° video databases (refer to Table 1), we focus primarily on authentic distortions, which manifest as intricate combinations of multiple visual artifacts that emerge during the creation of 360° videos (Ghadiyaram and Bovik, 2016). Fig. 4 shows the entire 360° video processing pipeline, illustrating that the creation of 360° videos consists of two steps: optical acquisition using a multi-camera rig and the stitching of multiple planar videos with limited and overlapping FoVs. Visual distortions from the optical acquisition typically result from a combination of factors such as scene complexity, lens imperfection, sensor limitation, and non-professional shooting. These distortions encompass under/over-exposure, out-of-focus and motion blurring, sensor noise, annoying shaky motion, flickering², jerkiness³, and floating⁴ (Zeng et al., 2014). Stitching distortions are mainly due to the limitation of

² Flickering generally refers to unwanted frequent luminance or chrominance changes along the temporal dimension.

³ Jerkiness appears when the temporal resolution is too low to catch up with the speed of moving objects, leading to discontinuous object motion.

⁴ Floating denotes the erroneously perceived motion in certain regions relative to their surrounding background, which should remain stationary or move consistently with the background.

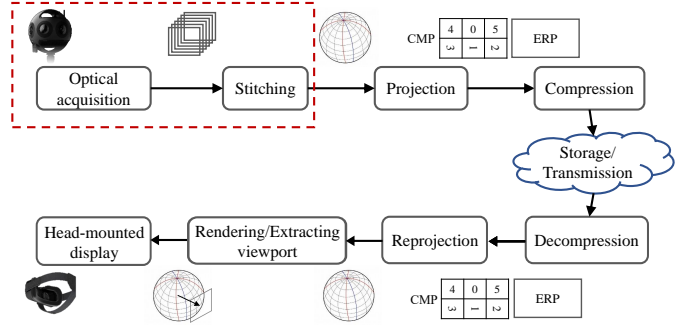


Fig. 4: 360° video processing pipeline, from optical acquisition to content consumption via an HMD. The optical acquisition and stitching are two main steps for 360° video creation, where authentic distortions arise.

the stitching algorithm itself and the stitching difficulty introduced by visual distortions from the previous acquisition step (e.g., stitching images of different luminance levels tends to create artificial boundaries, as shown in Fig. 5 (d)). Visually, stitching distortions are abrupt luminance/structure change, objects with missing parts, ghosting, and motion discontinuity localized in space and time. Of particular interest are the artificial converging points visible at the two poles (refer to Fig. 5 (h)). These authentic distortions inevitably affect the whole video processing pipeline and are ultimately perceived by end users.

3.1.2 Viewing Conditions

We use an HTC Eye Pro to display 360° videos, which offers an FoV of 110° and a binocular resolution of 2,880 × 1,600 pixels. Subjects are asked to seat on a swivel chair and wear the HMD to watch the videos. To collect EM and HM data, we employed the built-in Tobii Pro eye-tracking system with a sampling rate of 2×fps. Video playback is supported by a high-performance server with an AMD Ryzen 9 3950X 16-Core CPU, 128 GB RAM, and an NVIDIA GeForce RTX 2080 Ti GPU. The graphical user interface is customized using the Unity Game Engine.

An important consideration in our psychophysical experiment is the variation of two viewing conditions: the starting point and the exploration time. We intentionally choose **Starting Point I** to give users a *poor* initial viewing experience. This includes viewports that exhibit localized distortions or intensive spatiotemporal information. Another example is the initial viewport from the side when there is strong camera motion guidance. On the contrary, **Starting Point II** is selected to encourage a *good* initial viewing experience and is at least 120° (in longitude) away from Starting Point I. An

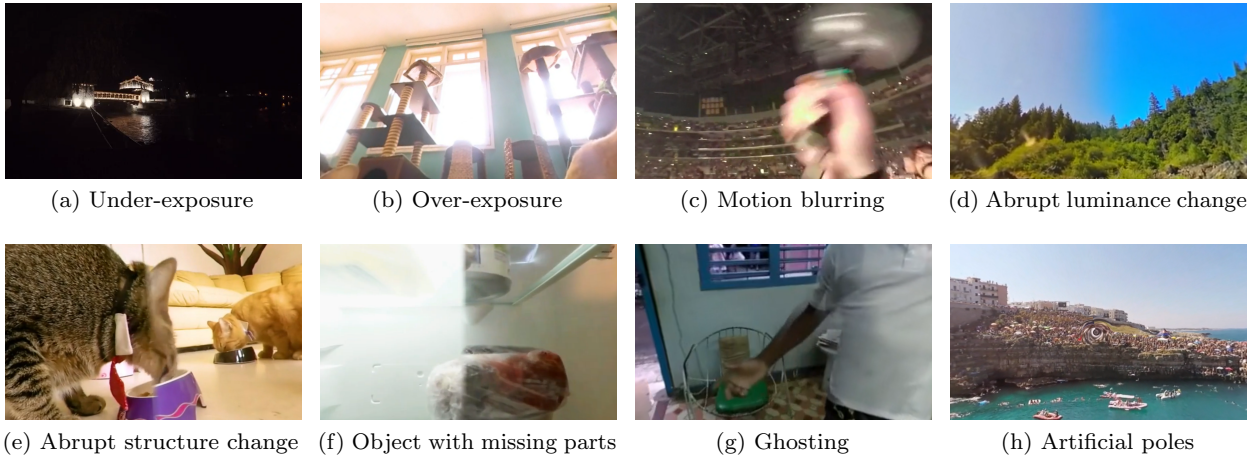


Fig. 5: Visual examples of authentic distortions in VRVQW.

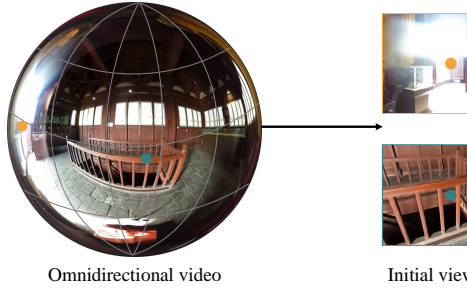


Fig. 6: We consider two types of starting points. Starting Point I (denoted by the light orange dot) and Starting Point II (denoted by the dark green dot) offer poor and good initial viewing experiences, respectively. The video name in VRVQW is “D_ConfucianTemple”.

example is shown in Fig. 6, where the viewport extracted from Starting Point I contains visible over-exposure and color cast distortions, while the viewport extracted from Starting Point II is of high quality. Additionally, we establish two exploration times: one spanning the entire duration (i.e., about 15 seconds) and the other set to half of the former (i.e., 7 seconds). Providing more exploration time allows for the extraction and viewing of more viewports. As shown in Fig. 7, the “F_BridgeOpening2” video captures a cruise ship sailing out of a dark cave. When viewing from Starting Point I during the first seven seconds, the user may encounter distortions like under-exposure and over-exposure, which can negatively impact her/his viewing experience. In the subsequent eight seconds, the cruise ship has sailed out of the cave, and the viewer may observe artifact-free high-quality content, which improves the viewing experience. By combining the starting point and exploration time, we create a total of four different viewing conditions.

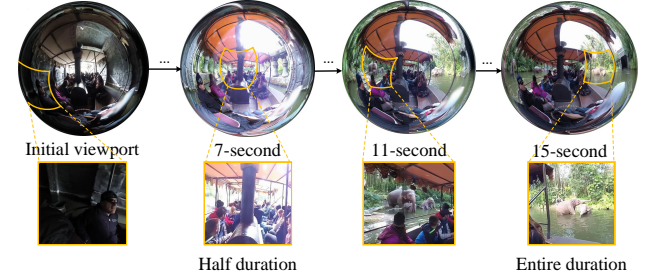


Fig. 7: We consider two exploration times, one spanning the entire duration (i.e., 15 seconds) and the other set to the half of the former (i.e., 7 seconds). The initial viewport is from Starting Point I. The video name in VRVQW is “F_BridgeOpening2”.

3.1.3 Subjective Methodology

The psychophysical study employs the single stimulus continuous quality evaluation method described in the ITU-R BT 500.13 recommendation (ITU, 2012). Subjects are required to rate the perceived quality of a 360° video on a continuous scale of [1, 5], labeled with five quality levels (“bad”, “poor”, “fair”, “good”, and “excellent”). To reliably collect MOSs, the experimental procedure consists of three phases: pre-training, training, and testing, as shown in Fig. 8.

In the *pre-training* phase, basic non-sensitive user information such as age, gender, and the requirement for wearing glasses are recorded. Subjects are familiarized with the experiment’s procedure and the rating guideline. We find it relatively time-consuming to teach subjects to use the hand controller for rating. Therefore, one of the authors is responsible for recording the opinion scores as they are read out by the subjects.

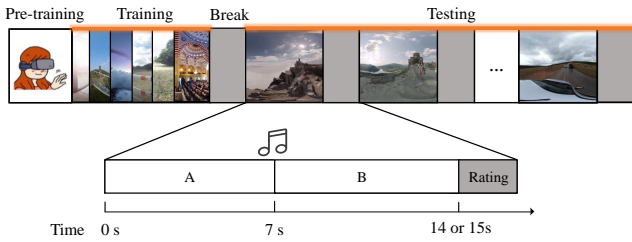


Fig. 8: Procedure of our psychophysical experiment. Period A: the first 7- second viewing. Period B: the second duration of viewing, separated by a voice prompt. After each video sequence is displayed, subjects need to give two scores, indicating their viewing experience in Period A, and both Periods A and B.

In the *training* phase, we select six video sequences that are not included in VRVQW. For the first four videos, subjects are allowed to freely explore the virtual scenes and are informed of the distortions they encounter during exploration. We find that this level of instruction is necessary to familiarize subjects with the distortions that are likely to occur in the testing phase. We try to avoid over-instructing the subjects, such as avoiding providing a reference MOS for each of the four videos. For the remaining two videos, we ask the subjects to give quality scores with no instructions. A discussion on how the subjects arrive at such ratings is held to make sure they understand the evaluation process. No feedback is provided on their scores. Importantly, if the subjects feel any discomfort during this phase, the experiment is interrupted immediately, and they are not invited to participate in the subsequent experiments.

In the *testing* phase, we divide the 502 videos into eight sessions to reduce fatigue and discomfort that may arise from possible long-time viewing. Additionally, the subjects are allowed to take a break at any time during this phase. Each session contains about 60 videos, with a 5-second mid-gray screen in between. We gather human data from 139 subjects (75 females and 64 males with ages between 17 and 26). All participants self-report normal or corrected-to-normal color vision. The subjects are divided into two groups according to two different sets of starting points. Each subject participates in at least two sessions, and each video is rated by no fewer than 20 subjects. We employ a well-established rating strategy described in (Sui et al., 2021; Duanmu et al., 2018) to collect MOSs for different exploration periods. Specifically, a voice prompt is played when the subject has viewed half of a 360° video (about 7 seconds) to remind her/him of giving a quality score based on the viewing experience so far. After completing the video, s/he is required to give another quality score according

to his/her overall viewing experience. It is noteworthy that each video is viewed only once by one subject to ensure that human data is collected without prior knowledge of the scene.

3.2 Data Processing

3.2.1 Human Opinion Scores

After obtaining the raw human scores, we detect and remove outliers using the method in (VQEG, 2000). We determine whether the subjective scores given to a 360° video are normally distributed by calculating the kurtosis coefficient:

$$\kappa = \frac{\mu_4}{(\sigma)^4}, \quad (1)$$

where μ_4 is the fourth central moment and σ is the standard deviation. If they are normally distributed (i.e., $\kappa \in [2, 4]$), an outlier is detected if the score is out of the range $[\mu - 2\sigma, \mu + 2\sigma]$. Otherwise, we extend the valid range to $[\mu - \sqrt{20}\sigma, \mu + \sqrt{20}\sigma]$ for outlier detection. Then, we compute the MOS by

$$q_j = \frac{1}{M} \sum_{i=1}^M q_j^{(i)}, \quad (2)$$

where $q_j^{(i)}$ is the opinion score of the i -th observer given to the j -th video sequence. In our study, each of the 502 videos in each viewing condition receives at least 20 ratings. Fig. 9 shows the MOSs with the corresponding 95% confidence intervals.

To validate the reliability of the collected MOSs in the less controllable VR viewing environment, we calculate the Pearson linear correlation coefficient (PLCC) between the ratings provided by an individual subject and the MOSs. Fig. 10 shows the correlation values obtained from 135 subjects (four subjects were detected as outliers), with a median correlation of 0.784, which is reasonably high compared to previous image/video quality databases with authentic distortions (Hosu et al., 2020; Ying et al., 2021). This result suggests that the adopted subjective rating strategy (with a voice prompt in between) is reliable for collecting MOSs in the VR environment.

3.2.2 Human Viewing Scanpaths

With the built-in eye-tracking system, we are able to gather both HM and EM data. The HM data for a subject is recorded in the form of a sequence of three Euler angles [pitch, yaw, roll]. Pitching up/down the head gives a positive/negative pitch value, in the range of

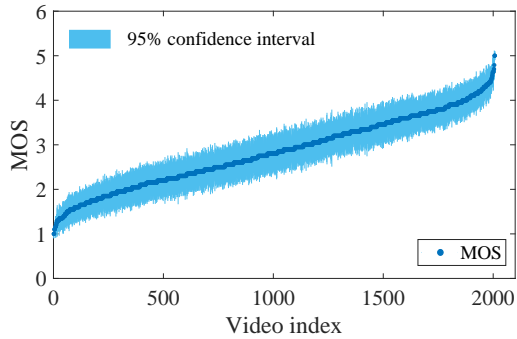


Fig. 9: MOSs (in the number of 502×4) with the corresponding 95% confidence intervals in VRVQW.

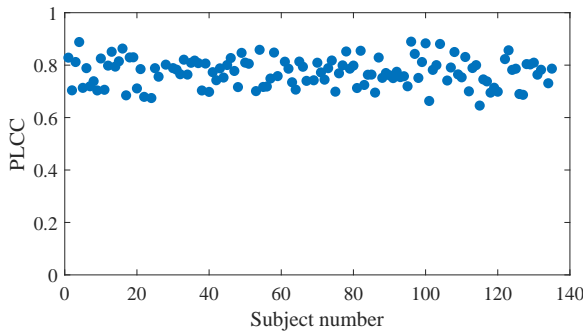


Fig. 10: Correlations between ratings from individual subjects and MOSs.

$[-90^\circ, 90^\circ]$; rotating the head to the left/right evokes a positive/negative **yaw** value, in the range of $[-180^\circ, 180^\circ]$; tilting the head to the left/right results in a positive/negative **roll** value. In the context of current VR HMDs, only the **pitch** and **yaw** values are relevant, corresponding to the center latitude and longitude coordinates of the extracted viewport. Similarly, the EM data for a subject is directly captured in the form of a sequence of **[longitude, latitude]**, representing the positions at which the eye is looking. The sampling rate for both HM and EM data is $2 \times$ fps, with a maximum frequency of 90 Hz constrained by the HMD. Compared to HM data, EM data tend to be noisier due to the alternating behavioral modes of attention and re-orientation (Sitzmann et al., 2018). Thus, we define the scanpath of a user as the sequence of **[pitch, yaw]** derived from the HM data.

4 Statistical Analysis of VR Data

4.1 Understanding Viewing Behaviors in VR

With the recorded data, we gather insights and investigate a number of questions about user behaviors when watching VR videos in the wild. In this study, we specifically concentrate on analyzing one particular type of viewing behaviors—the scanpath—because it has a significant impact on the perceived quality of a 360° video by the corresponding user.

4.1.1 Viewing Behavior Metrics

To compare multiple scanpaths, we adopt two widely used metrics: *temporal correlation* (Anderson et al., 2015) and *similarity ring metric* (Curcio et al., 2017a). We also consider comparing the saliency maps (i.e., the *heatmaps*) as spatial aggregations of the scanpaths for further analysis.

- *Temporal correlation* uses PLCC to calculate the correlations between the longitude values and the latitude values of two scanpaths, denoted as $s^{(i)} = [\phi^{(i)}, \theta^{(i)}]$ and $s^{(j)} = [\phi^{(j)}, \theta^{(j)}]$, followed by simple averaging:

$$TC(s^{(i)}, s^{(j)}) = \frac{1}{2} \left(PLCC(\phi^{(i)}, \phi^{(j)}) + PLCC(\theta^{(i)}, \theta^{(j)}) \right), \quad (3)$$

where $\phi^{(i)}$ and $\theta^{(i)}$ represent the longitudes and latitudes of the i -th scanpath, respectively. The mean temporal correlation over M subjects exploring the video is calculated by

$$mTC = \frac{2 \sum_{i=1}^{M-1} \sum_{j=i+1}^M TC(s^{(i)}, s^{(j)})}{M(M-1)}. \quad (4)$$

- *Similarity ring metric* measures whether different subjects have been watching the same parts of the video at the same time. While it is less likely for all scanpaths to completely overlap, it is reasonable to determine if they fall within a certain range, i.e., passing through the same *ring*. As suggested by (Curcio et al., 2017a), we focus on the longitude of the scanpath and set the radius and the center of the ring as $r = \text{FoV}/2$ and the mode of longitude values from M scanpaths at the same time instance:

$$c_t = \text{mode}(\phi_t^{(1)}, \phi_t^{(2)}, \dots, \phi_t^{(M)}). \quad (5)$$

A longitude value out of the ring means that the corresponding subject does not watch the same content with respect to other subjects at the t -th time

Table 2: Viewing behavior consistency in terms of mTC and SRM (and the associated standard error) under different viewing conditions.

| | | Starting Point I | Starting Point II |
|-----|-----------|------------------------|------------------------|
| mTC | 7-second | 0.394 (± 0.046) | 0.395 (± 0.041) |
| | 15-second | 0.289 (± 0.038) | 0.286 (± 0.034) |
| SRM | 7-second | 72.997 (± 7.221) | 74.702 (± 7.670) |
| | 15-second | 63.721 (± 5.371) | 65.128 (± 5.603) |

instance. The *instantaneous similarity* at the t -th time instance for the i -th scanpath is then defined as

$$IS_t^{(i)} = \begin{cases} 1, & \text{if } \phi_t^{(i)} \in \left[c_t - \frac{FoV}{2}, c_t + \frac{FoV}{2}\right], \\ 0, & \text{otherwise,} \end{cases} \quad (6)$$

based on which we compute the SRM by averaging across all scanpaths and over all time instances:

$$SRM = \frac{100}{MT} \sum_{t=1}^T \sum_{i=1}^M IS_t^{(i)}. \quad (7)$$

SRM is scaled to lie within $[0, 100]$, with a larger value indicating higher consistency.

– *Heatmap* reflects the salient areas to which users pay attention and can be considered as a spatial aggregation of the scanpaths. To generate dynamic heatmaps for omnidirectional videos, we apply the density-based spatial clustering (DBSCAN) algorithm (Ester et al., 1996) on the scanpaths of all subjects. Fixations are defined as the cluster centroids that span at least 200 ms (Chao et al., 2020), during which the gaze direction remains relatively unchanged. Noisy fixation points will be automatically filtered out. For every second of the video sequence, we compute a fixation map by DBSCAN. The saliency of each location in the fixation map is determined by the total spherical (i.e., great-circle) distances from the location to all fixation points (Xu et al., 2019), normalized by the computed maximum distance. To compare the similarity of two heatmaps, we follow (Sitzmann et al., 2018), and use PLCC as the quantitative measure.

4.1.2 Does the Viewing Condition Affect Viewing Behaviors?

To assess whether viewing behaviors are affected by the viewing conditions, we calculate mTC as defined in Eq. (4) and SRM as defined in Eq. (7) under different viewing conditions, as listed in Table 2. We also employ the analysis of variance (ANOVA) to see whether such

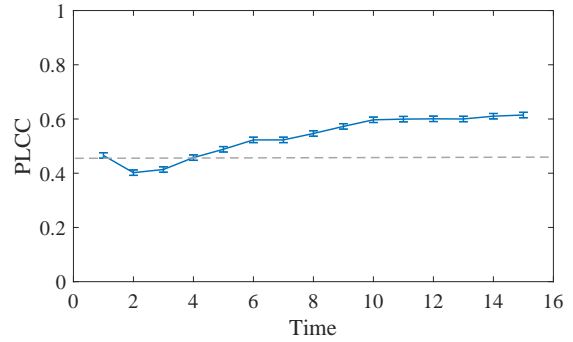


Fig. 11: Viewing behavior consistency in terms of PLCC between heatmaps from Starting Point I and Starting Point II, averaged over all 360° videos. The dashed line represents the initial PLCC.

Table 3: p -values in the ANOVA test for mTC and SRM. A p -value below the threshold of 0.05 represents that the corresponding factor has a significant impact on mTC and SRM, i.e., viewing behavior consistency.

| Factor | mTC | SRM |
|------------------|-------------|-------------|
| Starting point | 0.615 | ≈ 0 |
| Exploration time | ≈ 0 | ≈ 0 |

Table 4: Perceived quality analysis in terms of MOS (and the associated standard error) under different viewing conditions.

| | Starting Point I | Starting Point II |
|-----------|-----------------------|-----------------------|
| 7-second | 2.551 (± 0.034) | 3.059 (± 0.034) |
| 15-second | 3.119 (± 0.036) | 2.562 (± 0.038) |

differences in viewing behavior consistency as measured by mTC and SRM are statistically significant, as listed in Table 3. From the tables, we find that human viewing behavior consistency, as measured *globally* by mTC, is relatively low across all viewing conditions. However, when measured more *locally* by SRM, the consistency improves, and the differences in consistency for different starting points and exploration times are statistically significant, as evidenced by p -values close to zero.

Furthermore, we compute the mean PLCC values between the heatmaps from Starting Point I and Starting Point II, averaged over different videos, as shown in Fig. 11. We find that, within the first four seconds, the PLCC is lower than the initial, indicating divergent heatmaps, which can be explained by different viewing conditions. Second, the PLCC increases over time, but does not reach a sufficiently high level to eliminate the impact of viewing conditions.

Table 5: Perceived quality analysis in terms of MOS (and the associated standard error) under different video attributes.

| Video attribute | Average MOS |
|------------------|-----------------------|
| Low-resolution | 2.176 (± 0.024) |
| High-resolution | 3.081 (± 0.021) |
| No camera motion | 2.856 (± 0.021) |
| Camera motion | 2.779 (± 0.037) |

4.2 Understanding Perceived Quality in VR

Understanding how individuals perceive visual distortions in VR environments poses challenges due to the differences in viewing conditions between planar and immersive 360° videos. In this subsection, we analyze the effects of VR viewing conditions and video attributes on the perceived quality of omnidirectional videos.

4.2.1 Does the Viewing Condition Affect Perceived Quality?

Previous studies (Singla et al., 2017; Curcio et al., 2017b; Tran et al., 2017; Duan et al., 2017; Zhang et al., 2017, 2018a; Lopes et al., 2018; Li et al., 2018; Meng and Ma, 2022) assume that viewing conditions have a negligible impact on the perceived quality of 360° videos. This assumption holds true when considering *synthetic* artifacts (e.g., video compression) with *global* distortion appearances. In such cases, regardless of head orientation or any time instance, the extracted viewport is highly likely to contain the same main artifacts. However, this is not the case when it comes to VR videos in the wild, where we are dealing with *authentic* distortions, *localized* in space and time. Whether and when to encounter such spatiotemporal local distortions may have a different influence on the perceived quality. To test the hypothesis, we average the MOSs in VRVQW for different viewing conditions in Table 4. Several useful findings are worth mentioning. First, compared to a 15-second exploration, a 7-second exploration allows for fewer viewports of the scene to be observed, highlighting the importance of the starting point to the perceived video quality. Second, when longer exploration time is allowed, viewports closer to the end of the video exert a greater influence on the overall viewing experience due to the *recency effect* (Hands and Avons, 2001). This explains why, for the 7-second exploration, subjects tend to give low-quality scores when viewing from Starting Point I, where distortions appear in the initial viewports (see Sec. 3.1 for the definitions of the two types of starting points). Given more time, the subjects would consciously re-orient their heads to avoid viewing dis-

Table 6: The results of the multi-factorial ANOVA test for the effects of the starting point, the exploration time, the spatial resolution, and the camera motion on the *perceived quality*. *SS*: sum of squares. *d.f.*: degrees of freedom. *MS*: mean square. *F*: *F*-value. *p*: *p*-value for the null hypothesis. We omit three- and four-factorial analysis results, which are statistically insignificant.

| Source of variation | SS | d.f. | MS | F | p |
|---------------------|----------|------|---------|--------|-------------|
| Starting point | 1.600 | 1 | 1.604 | 3.560 | 0.059 |
| Exploration time | 0 | 1 | 0.004 | 0.010 | 0.927 |
| Spatial resolution | 207.250 | 1 | 207.250 | 459.79 | ≈ 0 |
| Camera motion | 0.200 | 1 | 0.201 | 0.450 | 0.505 |
| Starting point | 71.360 | 1 | 71.362 | 158.32 | ≈ 0 |
| Exploration time | | | | | |
| Starting point | 0.300 | 1 | 0.295 | 0.650 | 0.419 |
| Spatial resolution | | | | | |
| Starting point | 0.720 | 1 | 0.716 | 1.590 | 0.208 |
| Camera motion | | | | | |
| Exploration time | 0.110 | 1 | 0.105 | 0.230 | 0.629 |
| Spatial resolution | | | | | |
| Exploration time | 0.890 | 1 | 0.888 | 1.970 | 0.161 |
| Camera motion | | | | | |
| Spatial resolution | 3.750 | 1 | 3.746 | 8.310 | 0.004 |
| Camera motion | | | | | |
| Error | 897.900 | 1992 | 0.451 | | |
| Total | 1386.140 | 2007 | | | |

torted viewports and seek those with better quality, leading to an improved viewing experience. On the contrary, from Starting Point II, where the distortions may not be viewed initially, the subjects are less likely to observe distortions within the limited exploration time, thus explaining the higher average MOS of the 7-second exploration.

4.2.2 Does the Video Attribute Affect Perceived Quality?

We consider two video attributes: camera motion and spatial resolution. The camera motion is typically generated by body-mounted cameras. We carefully select 32 videos featuring complex camera motion (e.g., camera mounted on the roller coaster or held by a surfer). From Table 5, we find, as expected, that videos with camera motion generally receive lower MOSs regardless of the viewing conditions. This validates that using camera motion as strong visual guidance often results in annoying shaky motion, impairing the user viewing experience. We also show in Table 5 that high-resolution videos receive a higher average MOS than low-resolution ones (for all viewing conditions), even after being downsampled in the HMD. It remains to be determined whether such downsampling has a positive impact on the perceived quality by “concealing” certain types of distortions (e.g., compression artifacts and high-frequency noise).

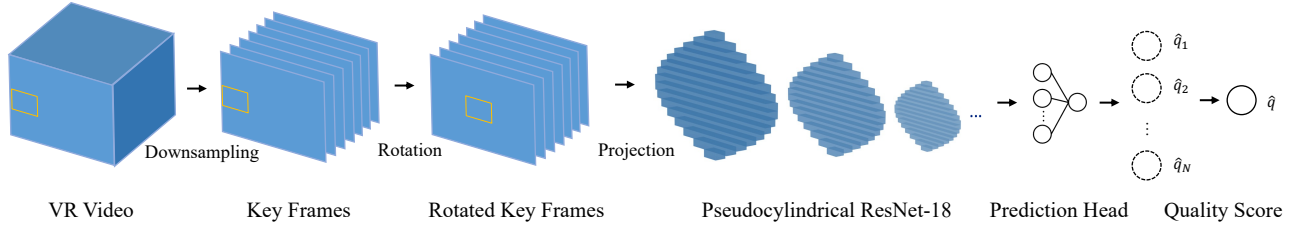


Fig. 12: System diagram of the proposed VR VQA model. Our model consists of four components: 1) a preprocessor for spatiotemporal downsampling and rotation, accounting for the two viewing conditions, 2) a projector for ERP to pseudocylindrical representation conversion, mitigating geometric distortions by ERP, 3) a feature extractor implemented by a pseudocylindrical CNN for spatial feature analysis, and 4) a quality regressor to compute frame-level scores, followed by temporal pooling.

4.2.3 Significant Impact Analysis

To test the statistical significance of the four factors — the starting point, the exploration time, the spatial resolution, and the camera motion — on perceived quality, we apply the multi-factorial ANOVA to the MOSs among factors. The results are listed in Table 6, from which we confirm that spatial resolution is a significant *individual* factor. The effect of the camera motion alone is not statistically significant, partially due to the limited inclusion of such videos to avoid visual discomfort. The perceived quality of user-generated VR videos is determined by the combination of two viewing conditions (i.e., the starting point and the exploration time). Interestingly, spatial resolution and camera motion also interact with each other, contributing to the overall perceived quality.

5 Objective Quality Assessment of VR Videos in the Wild

In this section, we describe a blind VQA model that 1) accounts for the two viewing conditions (i.e., the starting point and the exploration time), 2) respects the spherical nature of VR videos, 3) delivers accurate quality prediction performance, and 4) is computationally efficient.

5.1 Overview on Model Challenges

To the best of our knowledge, there is currently no objective VQA model specifically designed for VR videos in the wild. Such a proper quality model must address several key issues, including:

- *Spatial Resolution.* VR videos encompass the entire $360^\circ \times 180^\circ$ FoV with high fidelity, resulting in an

exceedingly high spatial resolution. To accelerate computational prediction, it is necessary to consider spatial downsampling as one of the preprocessing steps. But, how should we determine the downsampling factor?

- *Frame Rate.* Similar to spatial resolution, a high frame rate is essential for VR videos to enhance the sense of presence and to minimize motion sickness. For computational reasons, should we also perform temporal downsampling to identify and operate solely on a set of key frames?
- *Viewing Condition.* Naïve application of planar VQA models to VR videos under different viewing conditions is problematic because the same video is accompanied by multiple MOSs, each associated with one viewing condition. How to naturally model viewing conditions is the key to the success of VR VQA in the wild, but is little investigated even in the case of planar VQA.
- *Spherical Geometry.* VR videos are typically stored in ERP format, which introduces severe geometric distortions, especially in the vicinity of poles. Thus, directly transferring planar IQA/VQA models may achieve suboptimal performance. Among many sphere-to-plane and plane-to-sphere projections, which one should be adopted in VR VQA?

5.2 Proposed Method

To confront the above-mentioned model design challenges, we describe a VR VQA model encompassing four basic building blocks: 1) a preprocessor, 2) a projector, 3) a feature extractor, and 4) a quality regressor. The system diagram of our method is illustrated in Fig. 12.

- *Preprocessor.* As mentioned earlier, VR videos often come with high resolutions and frame rates, which

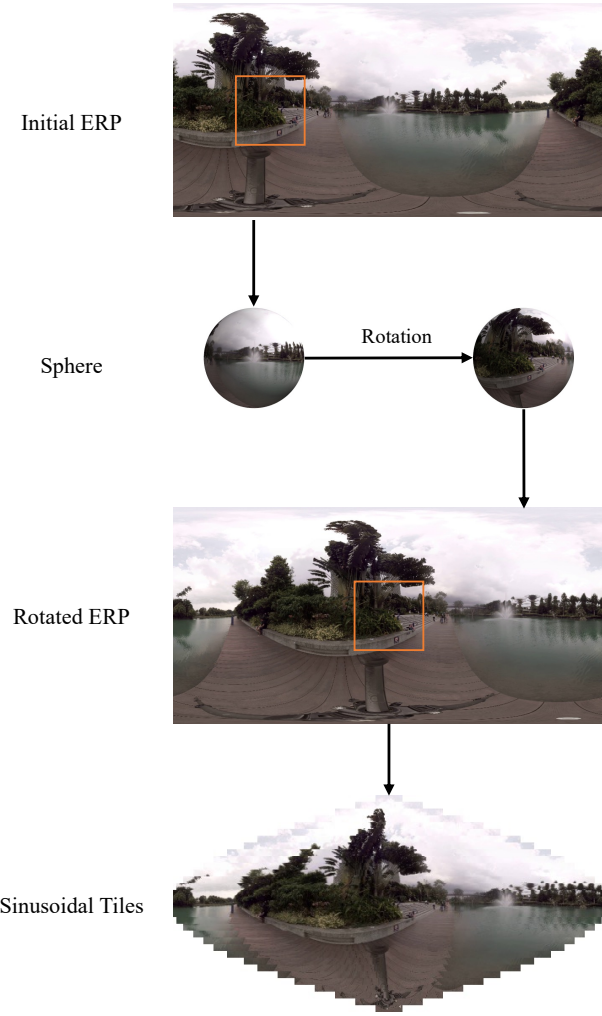


Fig. 13: Illustration of rotation and projection. We start by projecting an ERP frame onto a unit sphere, then rotating it to center the initial viewport specified by the starting point, and finally projecting it back to the ERP format. We then transform the rotated frame into a tiled sinusoidal representation as a special case of the pseudocylindrical representation. The video name in VRVQW is “A_Bay”.

desire spatiotemporal downsampling. Our computational analysis reveals that the spatial distortions occurring in VR videos are fairly visually stable under spatial downsampling, and do not affect subsequent feature extraction. Thus, bilinear interpolation is adopted to downsample the ERP frames to a spatial resolution of $1,024 \times 512$. For temporal downsampling, it can be leveraged to model the exploration time viewing condition. Specifically, we may set the temporal downsampling rate to be linearly proportional to the exploration time. In our settings, we choose to downsample the 7-second and 15-second

videos in VRVQW to 1 and 0.5 fps, both leading to 7 key frames per video. To accommodate the starting point as the second viewing condition, we rotate the starting point to $(\phi, \theta) = (0, 0)$ with the minimum geometric distortion in ERP, as illustrated in Fig. 13.

– *Projector*. According to Gauss’s Theorema Egregium, any projection from a sphere to a plane inherently introduces some distortions. Thus, it is preferable to perform computation directly on the sphere. However, spherical operators (e.g., spherical convolution) are often computationally intensive, making them less suitable for time-sensitive video applications like VQA. Recently, Li et al. (2021) proposed the pseudocylindrical convolution as an effective approximation to spherical convolution, while enjoying efficient implementation by standard 2D convolution. The pseudocylindrical convolution needs to operate on the so-called pseudocylindrical representation (Li et al., 2021). Here we adopt a special case of the pseudocylindrical representation—sinusoidal tiles (Yu et al., 2015a)—as the projection format. Assuming a VR video frame $x \in \mathbb{R}^{H \times W}$, where H and W represent the height and the width, respectively, we divide and scale x into S tiles (i.e., nonoverlapping rectangles, see Fig. 13), $\{x_i\}_{i=1}^S$, where $x_i \in \mathbb{R}^{H_i \times W_i}$, $H_i = H/S$, $W_i = \cos(\theta_i)W$, and θ_i is the (mean) latitude of the i -th tile.

– *Feature Extractor*. We choose a variant of ResNet-18 (He et al., 2016) pre-trained on ImageNet-1k (Deng et al., 2009) as the spatial feature extractor. We make minimal modifications to ResNet-18 by stripping the classification head and replacing all standard 2D convolution with pseudocylindrical convolution. To define the pseudocylindrical convolution operation, we need to first specify the neighboring grid of $(u, v) \in \{1, \dots, H\} \times \{1, \dots, W\}$:

$$\mathcal{N} = \{(i, j) \mid i, j \in \{-K, \dots, K\}\}, \quad (8)$$

which is computed through the sphere-to-plane projection Li et al. (2021):

$$u_i = u + i, \quad (9)$$

$$v_j = \frac{W_{u_i}}{W_u}(v + 0.5) - 0.5 + \frac{\cos \theta_u}{\cos \theta_{u_i}} \frac{W_{u_i}}{W_u} j \quad (10)$$

$$= \frac{W_{u_i}}{W_u} \left(v + \frac{\cos \theta_u}{\cos \theta_{u_i}} j + 0.5 \right) - 0.5.$$

As u and u_i are close provided that H is large, we may assume $\cos(\theta_u) \approx \cos(\theta_{u_i})$ and simplify Eq. (10) to

$$v_j \approx \frac{W_{u_i}}{W_u}(v + j + 0.5) - 0.5, \quad (11)$$

from which we find that adjacent samples in a tile are just neighbors of one another. Moreover, searching for neighbors in an adjacent tile amounts to scaling it to the width of the current tile. This is referred to as pseudocylindrical padding Li et al. (2021). Pseudocylindrical convolution over sinusoidal tiles (or the more general pseudocylindrical representation) can be efficiently implemented by standard 2D convolution with pseudocylindrical padding. The adoption of pseudocylindrical convolution brings a significant advantage to the VR VQA model design: advanced model architectures as well as pre-trained weights for planar images and videos can be directly inherited with no modifications.

– *Quality Regressor*. After extracting the feature representation for each key frame, we adopt a linear prediction head to regress frame-level quality scores. The last step is to aggregate frame-level quality scores into an overall quality estimate. Among various temporal pooling strategies (Tu et al., 2020), we choose the simple average pooling.

6 Evaluating VQA Models on VRVQW

In this section, we compare the proposed VR VQA model with existing blind IQA/VQA models as well as two of its variants, as the performance “lower bound” and “upper bound”, respectively (see Fig. 14).

6.1 Model Selection

We select and adapt six blind IQA/VQA models, while noting that there is currently no blind VR VQA model for direct comparison.

1. NIQE (Mittal et al., 2013), the Natural Image Quality Evaluator, is a completely blind IQA model that does not rely on MOSs for training. NIQE measures the deviation of the test image from statistical regularities observed in natural undistorted images.
2. VSFA (Li et al., 2019b), the Video Semantic Feature Aggregation, is a blind VQA model with content-aware feature extraction and temporal memory modeling.
3. Li22 (Li et al., 2022), a two-stream CNN-based VQA model, leverages domain knowledge from spatial appearance and temporal motion through transfer learning. Li22 employs a pre-trained CNN for IQA to extract spatial features and a pre-trained CNN for action recognition to extract motion features. These features are fed into a quality regressor, guided by the

Spearman rank-order correlation coefficient (SRCC) and PLCC as the hybrid loss. Notably, Li22 sets the performance record for planar VQA.

4. MC360IQA (Sun et al., 2020), the Multi-Channel CNN for blind 360° IQA, uses six viewports covering the panoramic scene as input. Six parallel hyper-ResNet-34 networks (He et al., 2016) are used to extract features, which are then concatenated and fed into a quality regressor.
5. ERP-VQA, a special case of the proposed method, directly takes ERP frames as input, processed by ResNet-18 with standard 2D convolution. The pre-processor and the quality regressor remain the same. Conceptually, ERQ-VQA gives the performance “lower bound” for the proposed method.
6. Scanpath-VQA, another variant of the proposed method, extracts a set of 224×224 planar videos (corresponding to an FoV of $90^\circ \times 90^\circ$) by sampling, along users’ scanpaths, a number of viewports from the VR video. Since viewing behaviors under different viewing conditions are explicitly modeled, the pre-processor of Scanpath-VQA performs spatiotemporal downsampling only. The remaining processing for each extracted planar video is the same as ERP-VQA. The overall quality score is computed by averaging 2D video quality estimates:

$$\hat{q} = \frac{\sum_{i=1}^M \hat{q}^{(i)}}{M}, \quad (12)$$

where M is the number of scanpaths adopted for planar video extraction. On the positive side, Eq. (12) can be seen as a quality ensemble, which has the potential to boost the prediction performance. On the negative side, the computational complexity of Scanpath-VQA increases loosely by a factor of M , making it less practical when M is large. More importantly, Scanpath-VQA relies on the ground-truth scanpaths for quality computation, and thus provides the performance “upper bound” for our method.

6.2 Implementation Details

The implementations of all competing models are obtained from the original authors. For NIQE that does not require training, we compute per-ERP-frame quality score without spatiotemporal downsampling nor rotation, followed by simple average pooling. For VSFA and Li22, we re-train two separate models for two starting points in ERP domain without incorporating the pre-processor, and combine the results of the two models for evaluation. For MC360IQA as an end-to-end fine-tuned blind IQA model, we adopt the same pre-processor as

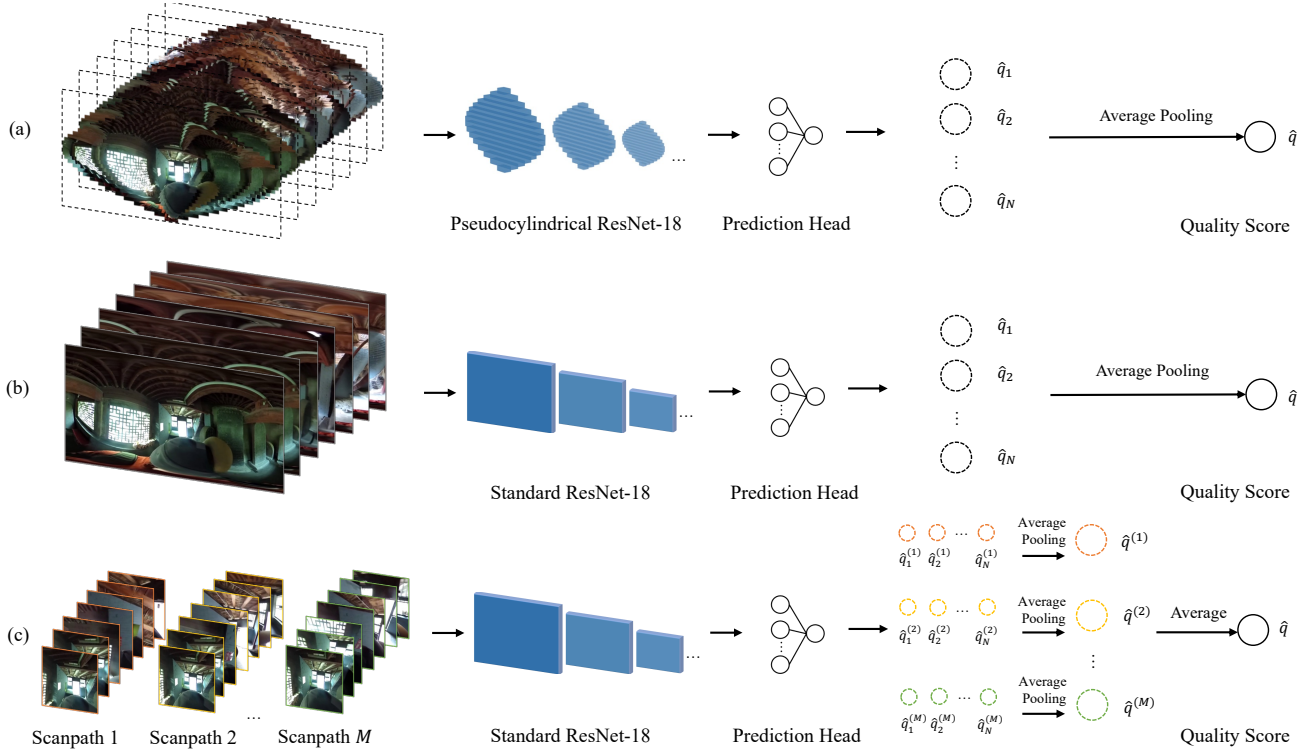


Fig. 14: Comparison of (a) the proposed method with its two variants: (b) ERP-VQA and (c) Scanpath-VQA. N represents the number of key frames after preprocessing. M represents the number of scanpaths used in Scanpath-VQA.

Scanpath-VQA, and re-train it on VRVQW by assigning the video-level quality score to each key frame. The temporally averaged score is utilized for testing. For ERP-VQA, Scanpath-VQA and the proposed method, all the learnable parameters are optimized for the PLCC loss using the Adam optimizer with a minibatch size of 8 and a learning rate of 5×10^{-5} for 30 epochs. The number of scanpaths, M , in Scanpath-VQA is set to 20, provided in VRVQW.

We randomly split VRVQW into three non-overlapping sets: 60% for training, 20% for validation, and 20% for testing. To avoid any bias caused by random partitioning, we repeat this process 10 times, and report the median results.

6.3 Performance Comparison

We summarize the PLCC and SRCC results in Table 7, from which we have several interesting observations. First, the model performance for Starting Point II is generally better than that for Starting Point I. This performance gap may be attributed to the fact that users from Starting Point I have higher chances of seeing

localized distortions, but the competing methods (including ours) may not accurately characterize these distortions, leading to an overestimation of the perceived quality. Such inaccuracy is more pronounced when the viewing time is shorter. Second, as expected, Scanpath-VQA sets the performance upper bound for all methods. Of particular interest is its comparison to MC360IQA, which essentially uses a set of synthetic still scanpaths for planar video extraction. The improved performance of Scanpath-VQA emphasizes the importance of incorporating ground-truth (or accurately predicted) users scanpaths into VR VQA. Third, our method ranks second, and consistently outperforms ERP-VQA, highlights the role of sinusoidal tiles (as a special case of the pseudocylindrical representation) and pseudocylindrical convolution to mitigate geometric distortions in ERP format and to construct effective VR VQA models. Fourth, the reasonable performance by VSFA is due primarily to the training of two separate models for different viewing conditions. When the training pipeline in the original paper is applied, the performance drops significantly. Nevertheless, its poorer performance compared to our method shows the necessity of end-to-end training/fine-tuning. Last but not least, it should be

Table 7: Performance comparison of different IQA/VQA methods on the proposed VRVQW under different viewing conditions. The top-2 results are highlighted in bold.

| Model | PLCC ↑ | | | | | | Overall | |
|--------------|------------------|--------------|-------------------|--------------|---------------------|--------------|--------------|--|
| | Starting Point I | | Starting Point II | | Starting Point I&II | | | |
| | 7s | 15s | 7s | 15s | 7s | 15s | | |
| NIQE | 0.322 | 0.417 | 0.409 | 0.388 | 0.348 | 0.393 | 0.371 | |
| VSFA | 0.720 | 0.809 | 0.825 | 0.814 | 0.694 | 0.792 | 0.746 | |
| Li22 | 0.780 | 0.842 | 0.858 | 0.881 | 0.664 | 0.520 | 0.508 | |
| MC360IQA | 0.734 | 0.778 | 0.760 | 0.799 | 0.653 | 0.676 | 0.669 | |
| ERP-VQA | 0.738 | 0.857 | 0.846 | 0.874 | 0.730 | 0.791 | 0.753 | |
| Scanpath-VQA | 0.782 | 0.874 | 0.836 | 0.858 | 0.785 | 0.789 | 0.783 | |
| Proposed | 0.755 | 0.868 | 0.860 | 0.881 | 0.738 | 0.794 | 0.761 | |

| Model | SRCC ↑ | | | | | | Overall | |
|--------------|------------------|--------------|-------------------|--------------|---------------------|--------------|--------------|--|
| | Starting Point I | | Starting Point II | | Starting Point I&II | | | |
| | 7s | 15s | 7s | 15s | 7s | 15s | | |
| NIQE | 0.350 | 0.455 | 0.461 | 0.429 | 0.387 | 0.428 | 0.407 | |
| VSFA | 0.694 | 0.791 | 0.824 | 0.813 | 0.684 | 0.788 | 0.750 | |
| Li22 | 0.764 | 0.830 | 0.853 | 0.859 | 0.642 | 0.505 | 0.438 | |
| MC360IQA | 0.738 | 0.771 | 0.762 | 0.798 | 0.652 | 0.675 | 0.672 | |
| ERP-VQA | 0.712 | 0.849 | 0.847 | 0.865 | 0.723 | 0.782 | 0.751 | |
| Scanpath-VQA | 0.772 | 0.865 | 0.813 | 0.850 | 0.785 | 0.787 | 0.781 | |
| Proposed | 0.730 | 0.862 | 0.859 | 0.872 | 0.737 | 0.784 | 0.757 | |

Table 8: Inference time in seconds of different VR VQA methods on a 15-second VR video with a resolution of 3,840 × 1,920 and a frame rate of 30 fps.

| Model | Inference Time |
|--------------|----------------|
| ERP-VQA | 4.09 |
| Scanpath-VQA | 173.77 |
| Proposed | 4.14 |

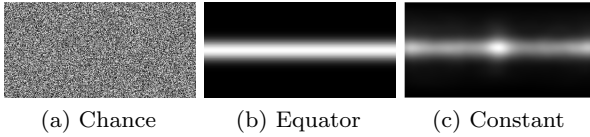


Fig. 15: Visualization of three saliency detection baselines.

stressed that even Scanpath-VQA, allowing the use of ground-truth scanpaths, cannot consistently provide the best performance across all viewing conditions, indicating ample opportunities to further advance blind VR VQA.

We further compare the inference time of our method against its two variants: ERP-VQA and Scanpath-VQA in Table 8. It is clear that the added computational complexity of pseudocylindrical convolution over standard 2D convolution is marginal. In contrast, Scanpath-VQA needs to evaluate and average the visual quality of multiple planar videos from different scanpaths, which is the slowest.

7 Evaluating Saliency Detection Models for VR Videos

In this section, we investigate the additional use of the proposed VRVQM for evaluating panoramic saliency detection models.

7.1 Model Selection

We choose three baselines and four state-of-the-art saliency detectors for evaluation.

1. Chance model assigns a uniformly distributed value from [0, 1] to each pixel in the heatmap (see Fig. 15 (a)).
2. Equator model consists of a symmetric Gaussian around the equator with a variance to cover 20% of the equator in the θ -direction and a degenerate Gaussian with infinite variance in the ϕ -direction (see Fig. 15 (b)).
3. Constant model is the average heatmap across the whole database (see Fig. 15 (c)).
4. PanoSalNet (Nguyen et al., 2018) employs transfer learning to adapt an existing saliency model (Simonyan and Zisserman, 2015) for ERP-based saliency detection. A prior filter that encodes inductive viewing biases (e.g., center and equator biases) is used to refine the prediction.
5. CP360 (Cheng et al., 2018) is a cubemap-based weakly-supervised model with a cube padding trick to reduce projection distortions and image border discontinuities.

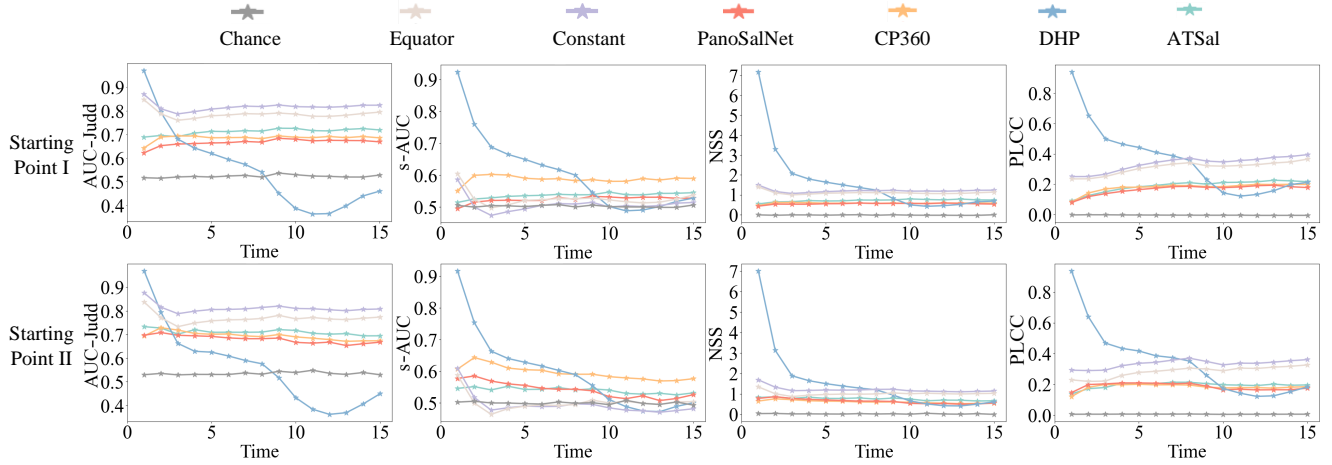


Fig. 16: Saliency detection performance changes over time for different starting points.

6. DHP (Xu et al., 2019) applies M workflows in parallel to predict the HM positions of M subjects for a 360° video. We set $M = 20$, which is the number of subjects in VRVQW. For each video frame, a heatmap can be obtained by Gaussian blurring the estimated HM positions.
7. ATSal (Dahou et al., 2021) is a two-stream CNN model, where the ERP-based stream is dedicated to extracting global attention statistics, while the cubemap-based stream aims at learning local saliency features.

The implementations of the four panoramic saliency detectors are again obtained from the original authors, and tested with the default settings.

7.2 Performance Comparison

We use four metrics to evaluate the saliency detection performance, including the Judd variant of the area under curve (AUC-Judd) (Judd et al., 2012), shuffle-AUC (s-AUC) (Tatler, 2007), normalized scanpath saliency (NSS) (Peters et al., 2005), and PLCC (Le Meur et al., 2007). To avoid the over-sampling problem in ERP format when calculating the metrics, we uniformly sample 1,000 points on the sphere, whose saliency values can be retrieved from the corresponding heatmap of size 180×360 , as suggested by David et al. (2018).

We show the overall performance for different starting points in Table 9. To make the results more comparable and interpretable, for each metric, we compute the human consistency as a realistic upper bound for model performance (Bylinskii et al., 2019). Specifically, we first compare the fixations of two groups of M observers, where M varies from 1 to 10 (i.e., half of the total 20

observers). We then fit the 10 performance scores to a power function (i.e., $aM^b + c$), and predict the human performance as that of two groups of infinite observers (which is equal to c , for $b < 0$). We also take a closer look at the performance changes over time for different starting points in Fig. 16. We find that DHP (Xu et al., 2019), which explicitly models the viewing conditions, performs the best among all models in terms of s-AUC, NSS, and PLCC (see also Fig. 17). Moreover, the equator and constant models confirm the effectiveness of the *equator bias* and are even among top-2 performers under AUC-Judd. Nevertheless, there is significant room for improvement as evidenced by the large performance gap between computational models and humans.

8 Conclusion and Discussion

We have put together VRVQW, the first in the wild VR video database that includes MOSs and viewing behavioral data. We conducted a psychophysical experiment on VRVQW, involving 139 users viewing VR videos from two conditions, resulting in a total of 40,268 opinion scores and scanpaths. We performed a statistical analysis of various effects on viewing behaviors and perceived quality in VR, identifying viewing conditions to be crucial. Furthermore, we proposed the first blind VQA model for VR videos, which demonstrates the state-of-the-art performance on VRVQW. We last evaluated several saliency detection models on VRVQW, pointing out the current progress of saliency detection in VR.

While our work presents an initial effort to understand the perceived quality of VR videos in the wild, there are still many important research problems that

Table 9: Performance comparison of different panoramic saliency detection models under different viewing conditions.

| | AUC-Judd \uparrow | | | s-AUC \uparrow | | | NSS \uparrow | | | PLCC \uparrow | | |
|------------|---------------------|-------------------|--------------|------------------|-------------------|--------------|------------------|-------------------|--------------|------------------|-------------------|--------------|
| | Starting Point I | Starting Point II | Overall | Starting Point I | Starting Point II | Overall | Starting Point I | Starting Point II | Overall | Starting Point I | Starting Point II | Overall |
| Chance | 0.523 | 0.535 | 0.529 | 0.502 | 0.500 | 0.501 | 0.018 | 0.024 | 0.021 | 0.005 | 0.006 | 0.006 |
| Equator | 0.784 | 0.769 | 0.777 | 0.525 | 0.501 | 0.513 | 1.103 | 1.015 | 1.059 | 0.309 | 0.283 | 0.296 |
| Constant | 0.815 | 0.811 | 0.813 | 0.507 | 0.494 | 0.501 | 1.203 | 1.206 | 1.205 | 0.336 | 0.334 | 0.335 |
| PanoSalNet | 0.665 | 0.680 | 0.673 | 0.523 | 0.541 | 0.532 | 0.546 | 0.639 | 0.593 | 0.165 | 0.185 | 0.175 |
| CP360 | 0.685 | 0.694 | 0.690 | 0.587 | 0.595 | 0.591 | 0.577 | 0.612 | 0.595 | 0.178 | 0.183 | 0.181 |
| DHP | 0.552 | 0.559 | 0.556 | 0.607 | 0.593 | 0.600 | 1.607 | 1.538 | 1.573 | 0.356 | 0.344 | 0.350 |
| ATSal | 0.711 | 0.711 | 0.711 | 0.536 | 0.540 | 0.538 | 0.714 | 0.753 | 0.734 | 0.188 | 0.194 | 0.191 |
| Human | 0.800 | 0.795 | 0.798 | 0.754 | 0.800 | 0.777 | 4.512 | 4.626 | 4.569 | 0.694 | 0.654 | 0.674 |

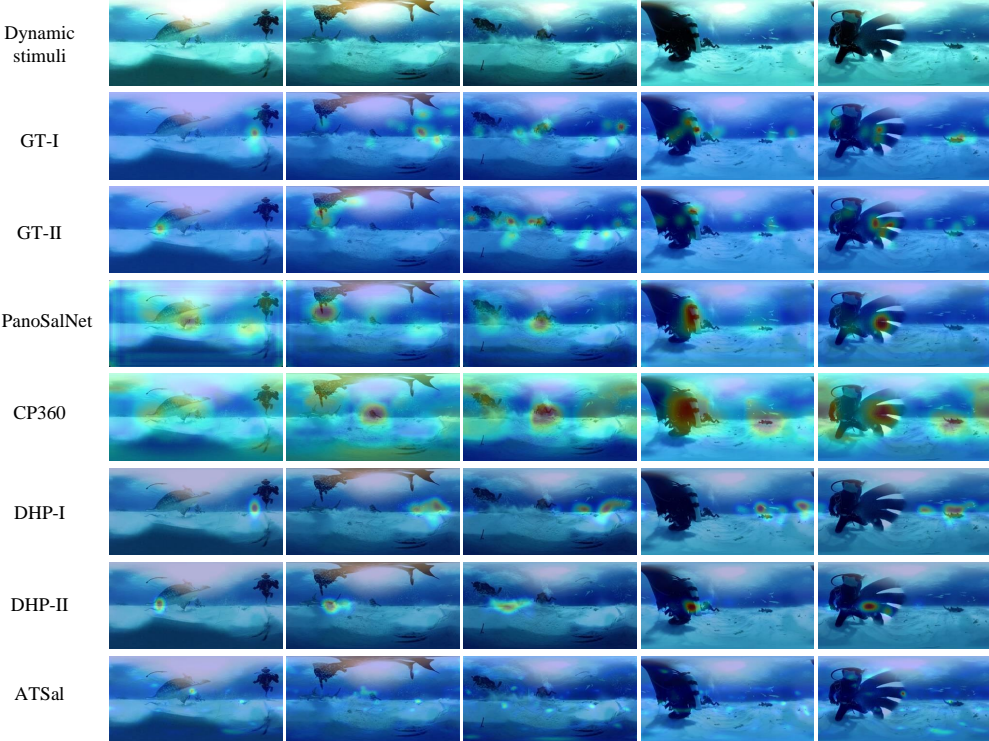


Fig. 17: Heatmaps produced by different saliency detection models. From left to right show the results of the 1-st, 4-th, 7-th, 10-th, and 15-th second, respectively.

remain unexplored. First, in our psychophysical experiment, we manually minimize the adverse physiological reactions by means of questionnaires. It would be interesting to design ingenious psychophysical experiments to disentangle visual discomfort and visual quality in a quantifiable way. Second, when collecting viewing behaviors, users are exposed to a VR scene only once in order to eliminate any prior knowledge of the scene configuration. However, it would be valuable to investigate how viewing behaviors change with repeated exposures to the same scene and how these changes impact the perceived quality of the scene. Third, objective quality models tailored to VR videos in the wild are largely lacking. Our study suggests that a key step in the model

development is the incorporation of viewing conditions. Scanpath-VQA that faithfully reflects how humans explore VR videos leads to improved performance. However, to fully automate Scanpath-VQA, scanpath prediction is inevitable, which is yet another challenging computational vision problem. Currently, the prediction of scanpaths for VR videos, particularly for long-term prediction (e.g., ≥ 10 seconds), is still a nascent area of research. Therefore, there is a need to develop more advanced scanpath prediction models that can provide accurate short-term and long-term predictions while also capturing the diverse nature of human scanpaths. Last but not least, the current work considers VR videos as the sole visual stimuli, it is of interest to investigate

audio-visual perception of VR videos (Chao et al., 2020) and its consequences on perceived quality.

References

Anderson NC, Anderson F, Kingstone A, Bischof WF (2015) A comparison of scanpath comparison methods. *Behavior Research Methods* 47(4):1377–1392

Azevedo RGdA, Birkbeck N, De Simone F, Janatra I, Adsumilli B, Frossard P (2020) Visual distortions in 360° videos. *IEEE Transactions on Circuits and Systems for Video Technology* 30(8):2524–2537

Bogdanova I, Bur A, Hugli H (2008) Visual attention on the sphere. *IEEE Transactions on Image Processing* 17(11):2000–2014

Bylinskii Z, Judd T, Oliva A, Torralba A, Durand F (2019) What do different evaluation metrics tell us about saliency models? *IEEE Transactions on Pattern Analysis and Machine Intelligence* 41(3):740–757

Chao FY, Ozcinar C, Wang C, Zerman E, Zhang L, Hamidouche W, Deforges O, Smolic A (2020) Audio-visual perception of omnidirectional video for virtual reality applications. In: *IEEE International Conference on Multimedia Expo Workshops*, pp 1–6

Chen S, Zhang Y, Li Y, Chen Z, Wang Z (2018) Spherical structural similarity index for objective omnidirectional video quality assessment. In: *IEEE International Conference on Multimedia and Expo*, pp 1–6

Cheng HT, Chao CH, Dong JD, Wen HK, Liu TL, Sun M (2018) Cube padding for weakly-supervised saliency prediction in 360° videos. In: *IEEE Conference on Computer Vision and Pattern Recognition*, pp 1420–1429

Cohen TS, Geiger M, Köhler J, Welling M (2018) Spherical CNNs. In: *International Conference on Learning Representations*, pp 1–15

Corbillon X, De Simone F, Simon G (2017) 360-Degree video head movement dataset. In: *ACM on Multimedia Systems Conference*, pp 199–204

Curcio IDD, Toukomaa H, Naik D (2017a) 360-Degree video streaming and its subjective quality. In: *SMPTE Annual Technical Conference and Exhibition*, pp 1–23

Curcio IDD, Toukomaa H, Naik D (2017b) Bandwidth reduction of omnidirectional viewport-dependent video streaming via subjective quality assessment. In: *International Workshop on Multimedia Alternate Realities*, pp 9–14

Dahou Y, Tliba M, McGuinness K, O'Connor NE (2021) ATSal: An attention based architecture for saliency prediction in 360° videos. In: *International Conference on Pattern Recognition*, pp 305–320

David EJ, Gutiérrez J, Coutrot A, Da Silva MP, Callet PL (2018) A dataset of head and eye movements for 360° videos. In: *ACM Multimedia Systems Conference*, pp 432–437

Deng J, Dong W, Socher R, Li LJ, Li K, Li FF (2009) ImageNet: A large-scale hierarchical image database. In: *IEEE Conference on Computer Vision and Pattern Recognition*, pp 248–255

Duan H, Zhai G, Yang X, Li D, Zhu W (2017) IVQAD 2017: An immersive video quality assessment database. In: *International Conference on Systems, Signals and Image Processing*, pp 1–5

Duanmu Z, Ma K, Wang Z (2018) Quality-of-experience for adaptive streaming videos: An expectation confirmation theory motivated approach. *IEEE Transactions on Image Processing* 27(12):6135–6146

Ester M, Kriegel HP, Sander J, Xu X (1996) A density based algorithm for discovering density varied clusters in large spatial databases. In: *International Conference on Knowledge Discovery and Data Mining*, pp 226–231

Ghadiyaram D, Bovik AC (2016) Massive online crowd-sourced study of subjective and objective picture quality. *IEEE Transactions on Image Processing* 25(1):372–387

Graf M, Timmerer C, Mueller C (2017) Towards bandwidth efficient adaptive streaming of omnidirectional video over HTTP: Design, implementation, and evaluation. In: *ACM on Multimedia Systems Conference*, pp 261–271

Götz-Hahn F, Hosu V, Lin H, Saupe D (2021) KonVid-150k: A dataset for no-reference video quality assessment of videos in-the-wild. *IEEE Access* 9:72139–72160

Hands DS, Avons SE (2001) Recency and duration neglect in subjective assessment of television picture quality. *Applied Cognitive Psychology* 15(6):639–657

He K, Zhang X, Ren S, Sun J (2016) Deep residual learning for image recognition. In: *IEEE Conference on Computer Vision and Pattern Recognition*, pp 770–778

Hosu V, Lin H, Sziranyi T, Saupe D (2020) KonIQ-10k: An ecologically valid database for deep learning of blind image quality assessment. *IEEE Transactions on Image Processing* 29:4041–4056

Itti L, Koch C, Niebur E (1998) A model of saliency-based visual attention for rapid scene analysis. *IEEE Transactions on Pattern Analysis and Machine Intelligence* 20(11):1254–1259

ITU (2012) Methodology for the subjective assessment of the quality of television pictures. *Recommendation ITU-R BT 500-13*

Judd T, Durand F, Torralba A (2012) A benchmark of computational models of saliency to predict human fixations. In: MIT Technical Report

Kennedy RS, Lane NE, Berbaum KS, Lilienthal MG (1993) Simulator sickness questionnaire: An enhanced method for quantifying simulator sickness. *The International Journal of Aviation Psychology* 3(3):203–220

Kim HG, Lim HT, Lee S, Ro YM (2019a) VRSA Net: VR sickness assessment considering exceptional motion for 360° VR video. *IEEE Transactions on Image Processing* 28(4):1646–1660

Kim HG, Lim HT, Ro YM (2019b) Deep virtual reality image quality assessment with human perception guider for omnidirectional image. *IEEE Transactions on Circuits and Systems for Video Technology* 30(4):917–928

Korhonen J (2019) Two-level approach for no-reference consumer video quality assessment. *IEEE Transactions on Image Processing* 28(12):5923–5938

Le Meur O, Le Callet P, Barba D (2007) Predicting visual fixations on video based on low-level visual features. *Vision Research* 47(19):2483–2498

Lebreton P, Raake A (2018) GBVS360, BMS360, ProSal: Extending existing saliency prediction models from 2D to omnidirectional images. *Signal Processing: Image Communication* 69:69–78

Lebreton P, Fremerey S, Raake A (2018) V-BMS360: A video extention to the BMS360 image saliency model. In: *IEEE International Conference on Multimedia Expo Workshops*, pp 1–4

Li B, Zhang W, Tian M, Zhai G, Wang X (2022) Blindly assess quality of in-the-wild videos via quality-aware pre-training and motion perception. *IEEE Transactions on Circuits and Systems for Video Technology* 32(9):5944–5958

Li C, Xu M, Du X, Wang Z (2018) Bridge the gap between VQA and human behavior on omnidirectional video: A large-scale dataset and a deep learning model. In: *ACM Multimedia*, pp 932–940

Li C, Xu M, Jiang L, Zhang S, Tao X (2019a) Viewport proposal CNN for 360° video quality assessment. In: *IEEE Conference on Computer Vision and Pattern Recognition*, pp 10169–10178

Li D, Jiang T, Jiang M (2019b) Quality assessment of in-the-wild videos. In: *ACM Multimedia*, pp 2351–2359

Li M, Ma K, Li J, Zhang D (2021) Pseudocylindrical convolutions for learned omnidirectional image compression. *arXiv preprint arXiv:211213227*

Lopes F, Ascenso J, Rodrigues A, Queluz MP (2018) Subjective and objective quality assessment of omnidirectional video. In: *Applications of Digital Image Processing*, pp 249–265

Meng Y, Ma Z (2022) Viewport-based omnidirectional video quality assessment: Database, modeling and inference. *IEEE Transactions on Circuits and Systems for Video Technology* 32(1):120–134

Mittal A, Soundararajan R, Bovik AC (2013) Making a ‘completely blind’ image quality analyzer. *IEEE Signal Processing Letters* 20(3):209–212

Nguyen A, Yan Z, Nahrstedt K (2018) Your attention is unique: Detecting 360-degree video saliency in head-mounted display for head movement prediction. In: *ACM Multimedia*, pp 1190–1198

Peters RJ, Iyer A, Itti L, Koch C (2005) Components of bottom-up gaze allocation in natural images. *Vision Research* 45(18):2397–2416

Simonyan K, Zisserman A (2015) Very deep convolutional networks for large-scale image recognition. In: *International Conference on Learning Representations*

Singla A, Fremerey S, Robitzsch W, Lebreton P, Raake A (2017) Comparison of subjective quality evaluation for HEVC encoded omnidirectional videos at different bit-rates for UHD and FHD resolution. In: *ACM Multimedia Workshops*, pp 511–519

Sitzmann V, Serrano A, Pavel A, Agrawala M, Gutierrez D, Masia B, Wetzstein G (2018) Saliency in VR: How do people explore virtual environments? *IEEE Transactions on Visualization and Computer Graphics* 24(4):1633–1642

Sui X, Ma K, Yao Y, Fang Y (2021) Perceptual quality assessment of omnidirectional images as moving camera videos. *IEEE Transactions on Visualization and Computer Graphics* 28(8):3022–3034

Sun W, Min X, Zhai G, Gu K, Duan H, Ma S (2020) MC360IQA: A multi-channel CNN for blind 360-degree image quality assessment. *IEEE Journal of Selected Topics in Signal Processing* 14(1):64–77

Sun Y, Lu A, Yu L (2017) Weighted-to-spherically-uniform quality evaluation for omnidirectional video. *IEEE Signal Processing Letters* 24(9):1408–1412

Tatler BW (2007) The central fixation bias in scene viewing: Selecting an optimal viewing position independently of motor biases and image feature distributions. *Journal of Vision* 7(14):1–17

Tran HTT, Ngoc NP, Bui CM, Pham MH, Thang TC (2017) An evaluation of quality metrics for 360 videos. In: *International Conference on Ubiquitous and Future Networks*, pp 7–11

Tu Z, Chen CJ, Chen LH, Birkbeck N, Adsumilli B, Bovik AC (2020) A comparative evaluation of temporal pooling methods for blind video quality assessment. In: *IEEE International Conference on Image Processing*, pp 141–145

VQEG (2000) Final report from the video quality experts group on the validation of objective models of

video quality assessment. In: Video Quality Experts Group Meeting

Wang Y, Jiang T, Ma S, Gao W (2012) Novel spatio-temporal structural information based video quality metric. *IEEE Transactions on Circuits and Systems for Video Technology* 22(7):989–998

Wang Z, Lu L, Bovik AC (2004) Video quality assessment based on structural distortion measurement. *Signal Processing: Image Communication* 19(2):121–132

Winkler S (2012) Analysis of public image and video databases for quality assessment. *IEEE Journal of Selected Topics in Signal Processing* 6(6):616–625

Wu C, Tan Z, Wang Z, Yang S (2017) A dataset for exploring user behaviors in VR spherical video streaming. In: *ACM on Multimedia Systems Conference*, pp 193–198

Xu J, Zhou W, Chen Z (2021) Blind omnidirectional image quality assessment with viewport oriented graph convolutional networks. *IEEE Transactions on Circuits and Systems for Video Technology* 31(5):1724–1737

Xu M, Song Y, Wang J, Qiao M, Huo L, Wang Z (2019) Predicting head movement in panoramic video: A deep reinforcement learning approach. *IEEE Transactions on Pattern Analysis and Machine Intelligence* 41(11):2693–2708

Xu M, Chen J, Wang H, Liu S, Li G, Bai Z (2020) C3DVQA: Full-reference video quality assessment with 3D convolutional neural network. In: *IEEE International Conference on Acoustics, Speech and Signal Processing*, pp 4447–4451

Ying Z, Mandal M, Ghadiyaram D, Bovik AC (2021) Patch-VQ: ‘Patching Up’ the video quality problem. In: *IEEE Conference on Computer Vision and Pattern Recognition*, pp 14019–14029

Yu M, Lakshman H, Girod B (2015a) Content adaptive representations of omnidirectional videos for cinematic virtual reality. In: *International Workshop on Immersive Media Experiences*, pp 1–6

Yu M, Lakshman H, Girod B (2015b) A framework to evaluate omnidirectional video coding schemes. In: *IEEE International Symposium on Mixed and Augmented Reality*, pp 31–36

Zakharchenko V, Choi KP, Park JH (2016) Quality metric for spherical panoramic video. In: *Optics and Photonics for Information Processing*, pp 57–65

Zeng K, Zhao T, Rehman A, Wang Z (2014) Characterizing perceptual artifacts in compressed video streams. In: *Human Vision and Electronic Imaging XIX, SPIE*, pp 173–182

Zhang B, Zhao J, Yang S, Zhang Y, Wang J, Fei Z (2017) Subjective and objective quality assessment of panoramic videos in virtual reality environments. In: *IEEE International Conference on Multimedia Expo Workshops*, pp 163–168

Zhang Y, Wang Y, Liu F, Liu Z, Li Y, Yang D, Chen Z (2018a) Subjective panoramic video quality assessment database for coding applications. *IEEE Transactions on Broadcasting* 64(2):461–473

Zhang Z, Xu Y, Yu J, Gao S (2018b) Saliency detection in 360° videos. In: *European Conference on Computer Vision*, pp 488–503